Progress In Electromagnetics Research C, Vol. 108, 201–210, 2021

Compact CPW-Fed Asymmetric UWB Antenna with Sufficient WLAN-Band Rejection

Rahul K. Garg[1, *], Maroor V. D. Nair[1], Sarthak Singhal[2], and Raghuvir Tomar[1]

Abstract—A coplanar waveguide fed asymmetric rectangular antenna with sufficient WLAN band-rejection is presented for ultra-wideband applications. The antenna uses an asymmetric rectangular patch, modified feedline, and defected coplanar ground plane for obtaining ultra-wideband performance. An inverted-L shaped slit in the radiating patch is used for realizing the WLAN band-rejection. The antenna is designed on a 1.6 mm thick FR-4 substrate having an area of $12 \times 16\,\text{mm}^2$ ($0.169\lambda_L \times 0.225\lambda_L$). An impedance bandwidth of 11.49 GHz with a WLAN band-notch from 5.15–5.86 GHz is achieved. In addition to this, desirable radiation characteristics in terms of stable radiation patterns, peak realized gain of 4.5 dBi, and maximum total efficiency of 81% are achieved in the pass-band. In the notched-band, the peak gain and total efficiency reduce to -1.3 dB and 40%, respectively. Measured results agree well with simulated results. This antenna structure has fractional bandwidth of 115.18% and a bandwidth dimension ratio of 3029, which is comparable or better than that of similar structures available in the literature. The proposed antenna has desirable time-domain performance in terms of fidelity factor, group delay, isolation, and S_{21} phase.

1. INTRODUCTION

Present wireless technologies require high data rate communication with high security and reliability. These demands are fulfilled by using wideband antenna structures. The modern advancements in fabrication technology have led to the miniaturization of communication systems. Therefore, a new design challenge faced by antenna designers is in terms of antenna size without compromising the antenna performance [1, 2]. Small physical dimensions of the antenna allow monolithic microwave integrated circuit (MMIC) designers to integrate additional components in the chip design.

An antenna having absolute bandwidth $\geq$ 500 MHz or fractional bandwidth $\geq$ 20% can be considered as an ultra-wideband (UWB) antenna, according to the definition given by Federal Communication Commission (FCC) [3, 4]. In addition to this, FCC allocated the frequency spectrum 3.1–10.6 GHz for UWB unlicensed usage. This frequency spectrum contains the frequency bands of commercial applications like WLAN and WiMAX. The signals generated by these commercial applications cause interference to the UWB signals. To mitigate this interference, another challenge of creating a band-notch in the UWB antenna arises. Antennas with small physical dimensions, ultra-wide bandwidth, and built-in band-rejection capabilities are the key requirements of present-day wireless communication systems [5, 6]. In the published literature, several UWB antenna designs comprising different radiator geometries like circular, rectangular, elliptical, hexagonal, octagonal, fractal geometries, modified trident, and modified rectangular shapes with and without notch-bands have been proposed [7–23]. The band-rejection capabilities are achieved by using circular slots, inverted-U slots, coupling slots, defects in the ground plane, etc. In all the above-discussed structures, either the antenna dimensions are large or the absolute bandwidth is less.

Received 25 November 2020, Accepted 7 January 2021, Scheduled 15 January 2021

* Corresponding author: Rahul Kumar Garg (rahulkumargarg08@gmail.com).

[1] Department of Electronics and Communication Engineering, The LNM Institute of Information Technology, Jaipur, India.

[2] Department of Electronics and Communication Engineering, Malaviya National Institute of Technology, Jaipur, India.

In the present work, a new miniaturized UWB antenna with WLAN band-rejection capabilities is presented. The techniques of asymmetric tapering in the feed line and defected coplanar waveguide (CPW) ground plane are used to achieve the UWB characteristics. An inverted-L shaped slit is loaded on the radiator to generate WLAN band-rejection. The proposed antenna geometry is designed and analyzed by using commercially available CST-Microwave Studio Simulator. The antenna prototype is fabricated and tested. The performance of the proposed design is compared with other already reported similar designs, in terms of their size, percentage size reduction, bandwidth, and bandwidth dimension ratio (BDR). The performance of the proposed design is either comparable or better than that of already reported similar designs.

2. DESIGN DETAILS

Figure 1(a) shows the proposed antenna geometry with optimized dimensions. Commercially available FR-4 substrate of size $12 \times 16 \times 1.6\,\text{mm}^3$ is used. The design derivation stages are shown in Figure 1(b). The design starts with an asymmetric rectangular monopole fed by a microstrip feedline with conventional CPW ground planes. It is followed by feedline tapering, creation of defects in the ground plane, and loading of the radiator with a half wavelength long inverted-L shaped slit. The location of the slit is determined by analyzing the surface current distribution on the patch at the

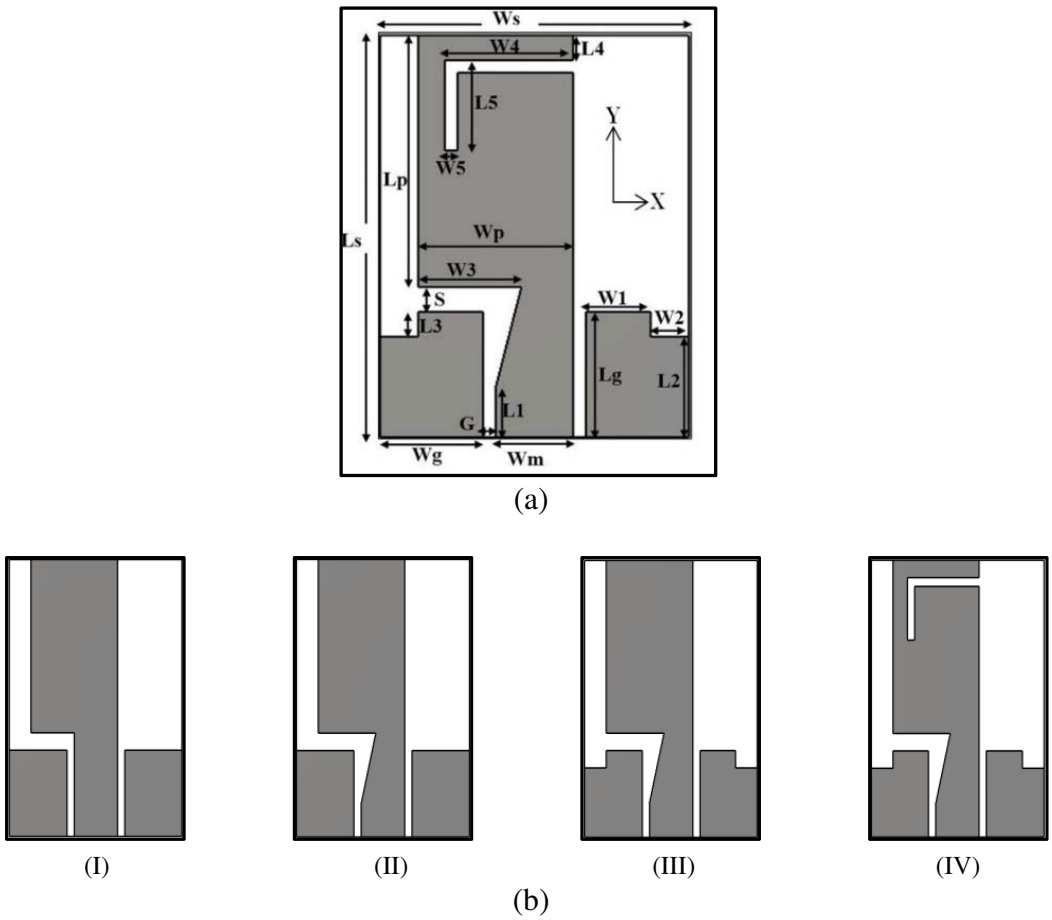

Figure 1. (a) Geometry of proposed antenna design (optimized design dimensions of the antenna are $Ws = 12\,\text{mm}$, $Wg = 4\,\text{mm}$, $Wp = 6\,\text{mm}$, $Wm = 3\,\text{mm}$, $W1 = 2.5\,\text{mm}$, $W2 = 1.5\,\text{mm}$, $W3 = 4\,\text{mm}$, $W4 = 5\,\text{mm}$, $W5 = 0.5\,\text{mm}$, $Ls = 16\,\text{mm}$, $Lg = 5\,\text{mm}$, $Lp = 10\,\text{mm}$, $L1 = 2\,\text{mm}$, $L2 = 4\,\text{mm}$, $L3 = 1\,\text{mm}$, $L4 = 1\,\text{mm}$, $L5 = 3.6\,\text{mm}$, $S = 1\,\text{mm}$, and $G = 0.5\,\text{mm}$). (b) Derivation stages: (I) Antenna-I, (II) Antenna-II, (III) Antenna-III, and (IV) Antenna-IV.

center of notched-band frequency. The length of the slit is calculated using Equation (1) [23].

$$L_{\text{slit}} = \frac{c}{2f_{\text{notch}}\sqrt{\frac{\varepsilon_r + 1}{2}}} \tag{1}$$

where $f_{\text{notch}} = 5.5\,\text{GHz}$, $L_{\text{slit}} = 2(W4 + L5) - W5 = 16.7\,\text{mm}$ (total electrical length of slit).

3. RESULTS AND DISCUSSIONS

3.1. Simulation Results

The variations of the reflection coefficient with frequency for the derivation stages are shown in Figure 2(a). For asymmetric rectangular monopole, i.e., Antenna-I, dual operating bands are achieved (4.72–7.99 GHz and 11.52–15.59 GHz). In Antenna-II, wideband characteristics are achieved by replacing the upper rectangular section of the feed line with a trapezoidal section. The impedance matching is also improved, resulting in wideband performance over the frequency spectrum of 4.49–14.52 GHz. This bandwidth improvement is achieved due to the smooth transition of higher-order modes from the feedline to the radiator. Thereafter, in the case of Antenna-III, designed by loading the ground planes with rectangular defects, further improvement in impedance matching leads to bandwidth enhancement from 10.03–10.83 GHz. In the last step, i.e., Antenna-IV, the loading of an inverted-L slit on the radiator results in rejection of the WLAN band (5.14–5.84 GHz). Besides this, an enhanced bandwidth of 11.49 GHz (4.23–15.72 GHz) is also achieved.

Figure 2(b) displays the surface current distribution at a few pass-band frequencies (4.8 GHz, 6.3 GHz, and 11.5 GHz) and stop-band frequency (5.5 GHz). It is observed that at the pass-band frequencies, the surface current is distributed across the different portions of the radiator, feedline, and ground planes based on the respective frequency. The non-concentration of the surface current at a particular portion results in good radiation in the pass-band. At the center frequency of notched-band

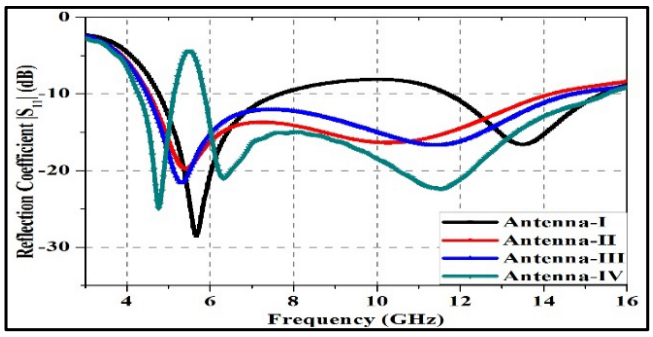

(a)

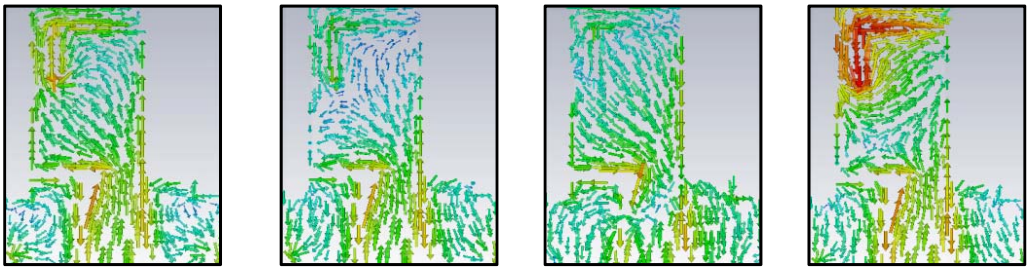

at 4.8 GHz at 6.3 GHz at 11.5 GHz at 5.5 GHz

(b)

Figure 2. (a) Reflection coefficient versus frequency performance plots for derivation stages. (b) Surface current distribution at pass-band and stop-band frequencies.

(i.e., 5.5 GHz), the surface current is confined to the inverted-L slit. This confinement of the surface current results in band-rejection at 5.5 GHz.

3.2. Characteristic Mode Analysis

The theory of characteristic mode (TCM) gives physical insight into the radiating modes of the antenna [24]. TCM analysis does not need any feed arrangement for the antenna. The only requirement is that lossless material should be used during the simulation process. TCM analysis results in performance parameters like eigenvalue, characteristic angle, and modal significance. Characteristic angle (Ψ) is related to the phase angle between characteristic current and related field whereas modal significance (Υ) is the normalized form of the eigenvalue (λ). These are calculated as follows in Eqs. (2)–(4) [24–29].

$$X(J_n) = \lambda_n R(J_n) \tag{2}$$

$$\Psi = 180^\circ - \tan^{-1}(\lambda_n) \tag{3}$$

$$\Upsilon = \left| \frac{1}{1 + j\lambda_n} \right| \tag{4}$$

where λ_n = Eigenvalue of the nth mode and J_n = Eigen current of the nth mode, and X and R are the imaginary and real parts of impedance matrix.

Figures 3–5 present the characteristic mode parameters for the derivation stages. The values of λ, Ψ, and Υ for a radiating mode are 0, 180°, and 1, respectively. Table 1 lists the detailed results obtained for various characteristic mode parameters for all the derivation stages. It is observed that mode 1 and mode 2 are the radiating modes and mode 3 is the non-radiating mode.

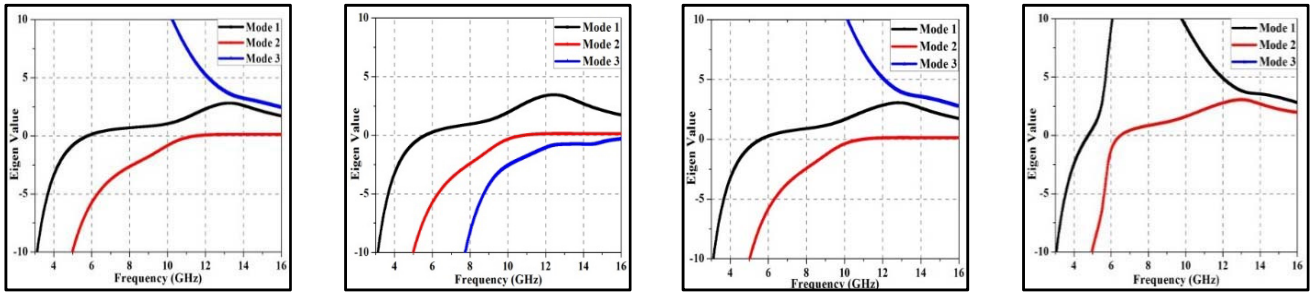

(a) Antenna-I (b) Antenna-II (c) Antenna-III (d) Antenna-IV

Figure 3. Eigenvalue (λ).

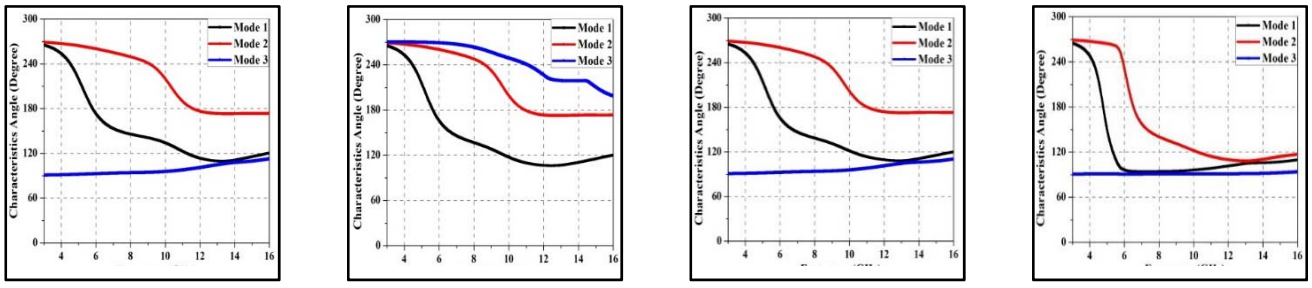

(a) Antenna-I (b) Antenna-II (c) Antenna-III (d) Antenna-IV

Figure 4. Characteristic angle (Ψ).

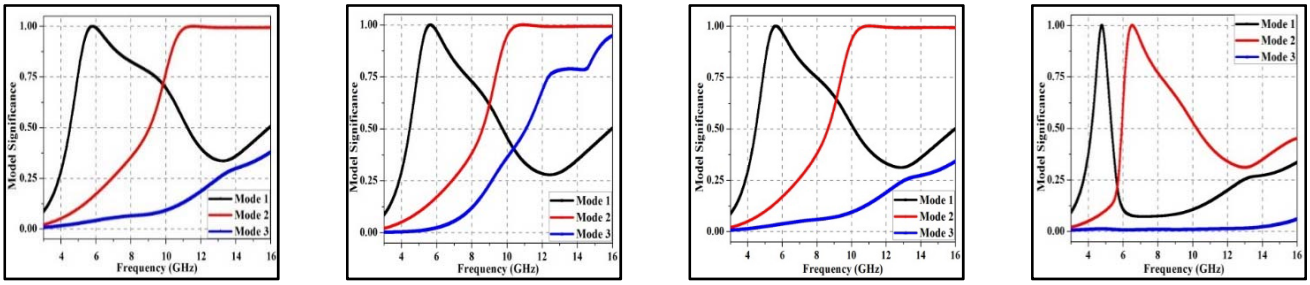

(a) Antenna-I (b) Antenna-II (c) Antenna-III (d) Antenna-IV

Figure 5. Modal significance (Υ).

Table 1. List of characteristic mode analysis parameters for derivation stages.

Sr. No.	Antenna	Resonating Mode	Resonant Frequency at		
			$\lambda = 0$	$\Psi = 180°$	$\Upsilon = 1$
1.	Antenna-I	Mode 1	5.81 GHz	5.81 GHz	5.81 GHz
		Mode 2	11.58 GHz	11.58 GHz	11.38 GHz
2.	Antenna-II	Mode 1	5.64 GHz	5.64 GHz	5.63 GHz
		Mode 2	10.91 GHz	10.91 GHz	10.8 GHz
3.	Antenna-III	Mode 1	5.62 GHz	5.62 GHz	5.62 GHz
		Mode 2	11.03 GHz	11.04 GHz	10.86 GHz
4.	Antenna-IV	Mode 1	4.77 GHz	4.77 GHz	4.81 GHz
		Mode 2	6.52 GHz	6.52 GHz	6.52 GHz

3.3. Measured Results

The antenna prototype and simulated and experimental reflection coefficients are illustrated in Figure 6(a). It is observed that the measured lower and upper cutoff frequencies of 4.27 GHz and 15.51 GHz are slightly different from the simulated values of 4.35 GHz and 15.35 GHz, respectively. The lower band edge frequency of the proposed UWB antenna is in accordance with the other similar structures [9–21]. Moreover, the simulated and measured notch-band frequency ranges are 5.14–5.84 GHz and 5.3–6.02 GHz, respectively. The value of the simulated and experimental reflection coefficient in the notched-band are −5.48 dB and −6.12 dB, respectively. These values of the reflection coefficient in notched-band are in accordance with those previously reported in structure available in literature [23]. Minor discrepancies between simulated and measured results can be attributed to the fabrication tolerances, effects of frequency on dielectric constant, etc. The realized gain and efficiency plots are shown in Figure 6(b). It is observed that the peak antenna gain, total efficiency, and radiation efficiency have their maximum of 4.5 dB, 81%, and 79%, respectively, in the pass-band. In the rejected-band, the peak gain decreases to −1.3 dB; total efficiency decreases to 40%; and radiation efficiency decreases to 39%.

Simulated and measured radiation patterns in both E-plane and H-plane at 4.7 GHz, 7 GHz, and 11.75 GHz are shown in Figure 7. At lower frequencies (< 10 GHz), dipole-like patterns in E-plane and omnidirectional patterns in H-plane are observed. For higher frequencies (> 10 GHz), due to higher mode excitation, distorted omnidirectional patterns in the E-plane and omnidirectional patterns in H-plane are observed.

Table 2 compares the proposed design with already published similar designs. The comparison is based on the dimensions of the antenna in terms of wavelength λ_L (calculated based on the lowest cutoff frequency of impedance bandwidth), percentage size reduction, absolute bandwidth, fractional

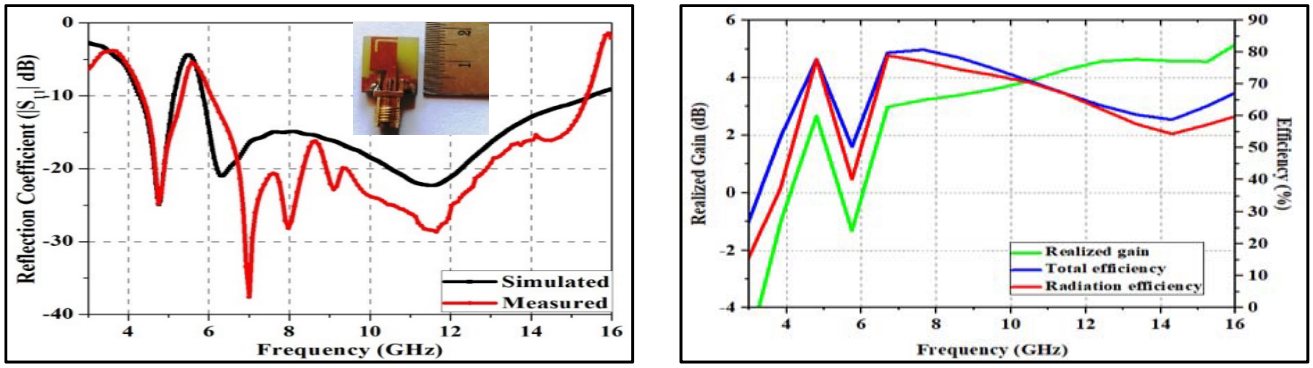

(a) (b)

Figure 6. (a) Photograph of fabricated antenna, simulated and measured reflection coefficient plot, and (b) realized gain and efficiency versus frequency plots.

Table 2. Comparison of the proposed design with other reported designs in the literature.

Sr. No.	Reference	Size ($\lambda_L \times \lambda_L$)	% Size reduction (in terms of λ_L^2)	Lower-Higher Frequency (GHz)	Bandwidth (GHz)	Fractional Bandwidth (%)	BDR
1.	[7]	0.99×1.34	97.13	4.4–17.6	13.2	120	90.45
2.	[8]	0.272×0.39	64.15	3.89–11.58	7.69	99.4	937.02
3.	[9]	1.516×1.516	98.35	4.55–13	8.45	96.29	41.89
4.	[10]	0.29×0.28	46.92	4.94–12.72	7.78	88.1	1085.08
5.	[11]	0.275×0.264	47.62	3.3–9	5.7	92.68	1276.58
6.	[12]	1.68×1.68	98.65	6–16	10	90.9	32.06
7.	[13]	0.47×0.41	80.26	4.06–6.34	2.28	43.84	227.53
8.	[14]	0.55×0.55	87.42	5.12–6.32	1.2	20.97	69.35
9.	[15]	0.72×0.72	92.66	4.31–6.78	2.47	44.54	85.92
10.	[16]	0.33×0.32	63.99	4–8.44	4.44	71.38	675.97
11.	[17]	0.97×0.795	95.06	5–7	2	33.3	43.22
12.	[18]	0.87×0.87	94.97	5.23–5.77	0.54	13.5	17.83
13.	[19]	0.382×0.382	73.94	4.25–12.5	8.25	98.5	675
14.	[20]	0.38×0.386	66.3	7.11–12.71	5.6	56.5	385.19
15.	[21]	0.576×0.576	88.53	4.32–6.3	1.98	37.28	112.38
16.	**Proposed**	$\mathbf{0.169 \times 0.225}$	-	**4.23–15.72**	**11.49**	**115.18**	**3029.05**

bandwidth, and BDR [10]. It is observed that the proposed antenna has a size reduction of $\sim 98\%$ over the previously reported designs. Moreover, the proposed antenna has a bandwidth of 11.49 GHz, fractional bandwidth of $\sim 115\%$, and BDR of ~ 3029. These performance parameter values indicate that the proposed antenna has the widest bandwidth, the largest value of BDR, and very high size miniaturization in comparison to other compared geometries.

4. TIME-DOMAIN ANALYSIS

In addition to frequency-domain analysis, time-domain analysis of the UWB antenna is also necessary to analyze the effect of an antenna on the time-domain pulse due to the large bandwidth. In this analysis, two identical proposed antenna geometries are placed 30 cm apart from each other (to ensure

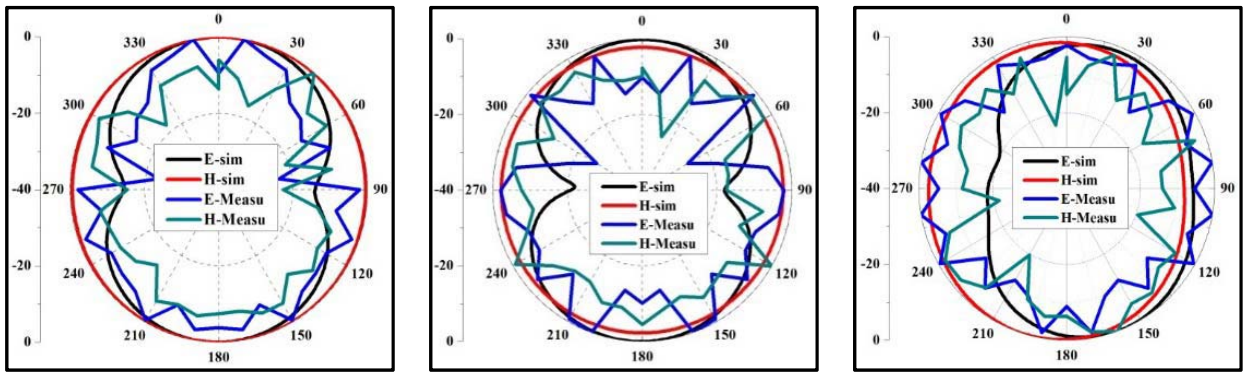

Figure 7. Simulated and measured radiation pattern at (a) 4.7 GHz, (b) 7 GHz, and (c) 11.75 GHz.

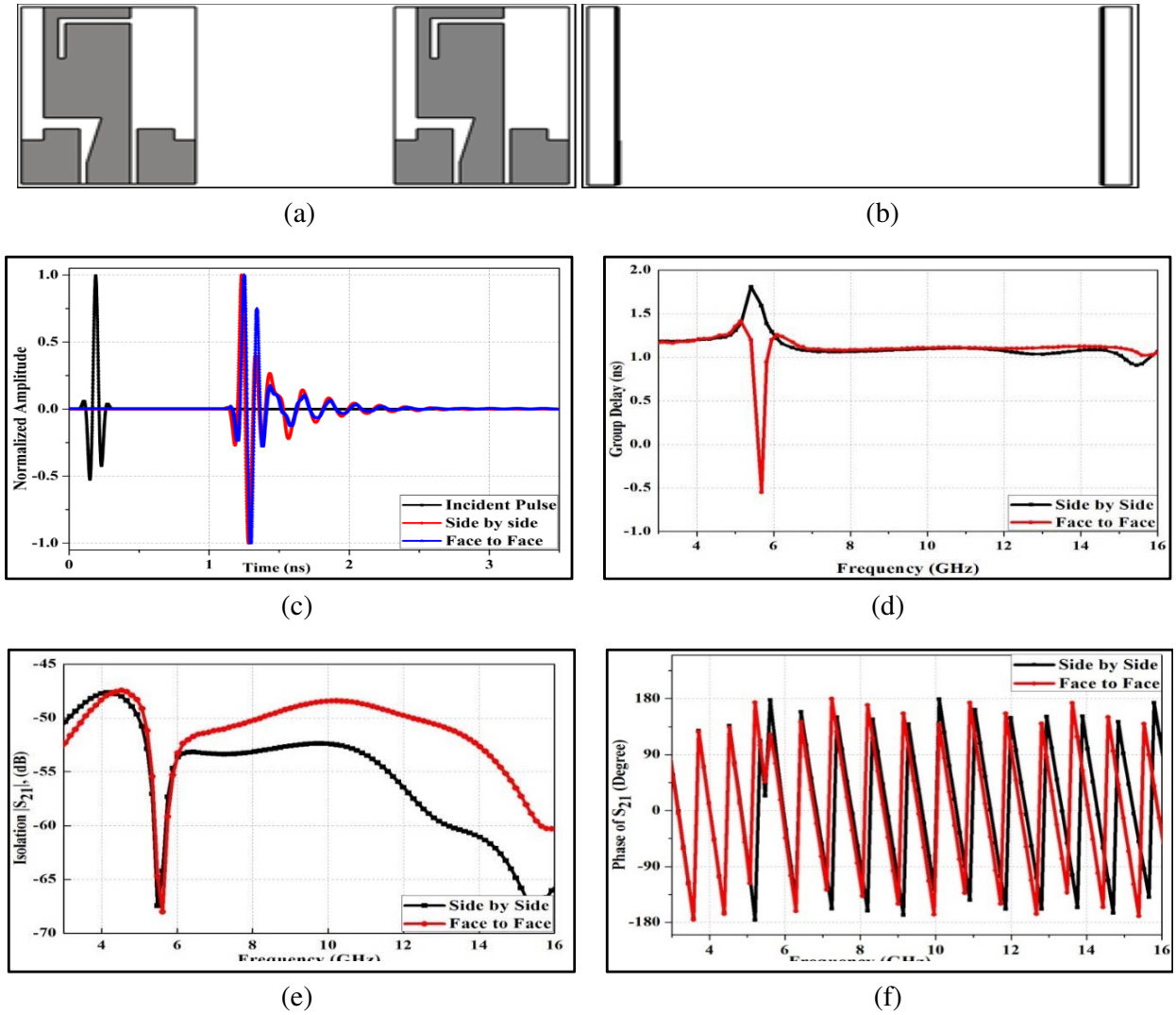

Figure 8. Time-domain analysis setup and performance parameters, (a) Face-to-Face (F2F) configuration, (b) Side-by-Side (S2S) configuration, (c) normalized transmitted and received pulse amplitudes, (d) group delay, (e) isolation magnitude, and (f) S_{21} phase.

the far-field condition) in two different configurations known as Face-to-Face (F2F) and RF Side-by-Side (S2S) configurations, as presented in Figures 8(a)–8(b). In each configuration, one antenna works as the transmitting antenna (which is excited by a short Gaussian pulse), and the other works as the receiving antenna [30]. Time-domain performance of the proposed UWB antenna in terms of transmitted and received pulse shapes, fidelity factor, group delay, isolation ($|S_{21}|$) magnitude, and S_{21} phase is shown in Figures 8(c)–8(f).

$$F = \max \left[\frac{\int_{-\infty}^{\infty} S_t(t) S_r(t+\tau) d\tau}{\int_{-\infty}^{\infty} |S_t(t)|^2 \, dt \int_{-\infty}^{\infty} |S_r(t)|^2 \, dt} \right] \tag{5}$$

where $S_t(t)$ = transmitted pulse, $S_r(t)$ = received pulse and τ = group delay.

Normalized amplitudes of the transmitted and received pulses are shown in Figure 8(c). The fidelity factor which represents the correlation between transmitted and received pulses (calculated using Equation (5)) is 94% in F2F configuration and 87% in S2S configuration. Group delay is almost constant in the entire frequency range except for the band-notch region where it varies from 1.5 ns to 2 ns. This group delay variation is within the permissible limit of 5 ns mentioned in the literature [30, 31]. In each configuration, isolation is better than 45 dB, and the isolation phase has an almost linear variation with frequency in the passband. This ensures the absence of undesired out-of-phase components over the entire operating band (excepting the nonlinear variations in notch-band).

5. CONCLUSIONS

A new type of compact ultra-wideband antenna with sufficient WLAN band-rejection is presented. Asymmetric rectangular monopole antenna with tapered feed-line and defected coplanar waveguide ground planes is used to enhance the bandwidth. An Inverted-L slit is loaded on the patch to reject the WLAN band. The prototype with optimized dimensions is simulated, fabricated, and tested. The measured data are in good agreement with the simulated data. This antenna design will find applications in many modern ultra-wideband communication systems.

ACKNOWLEDGMENT

The authors acknowledge the help and support provided by Government Women Engineering College, Ajmer, and convey sincere thanks to the organization.

REFERENCES

1. Schantz, H. G., "A brief history of UWB antennas," *IEEE Aerospace and Electronic Systems Magazine*, Vol. 19, No. 4, 22–26, 2004.
2. Wiesbeck, W., G. Adamiuk, and C. Sturm, "Basic properties and design principles of UWB antennas," *Proceedings of the IEEE*, Vol. 97, No. 2, 372–385, 2009.
3. Federal Communication Commission, "First-order and report: Revision of Part 15 of the commission's rules regarding UWB transmission systems," 2002.
4. Electronic Communication Committee (ECC), "The European table of frequency allocations and applications," ERC report 25, 2014.
5. Cicchetti, R., E. Miozzi, and O. Tesla, "Wideband and UWB antennas for wireless applications: A comprehensive review," *International Journal of Antennas and Propagation, Hindawi Publishing Corporation*, Vol. 2017, 1–45, 2017.
6. Kumar, G. and R. Kumar, "A survey on planar ultra-wideband antennas with band-notch characteristics: Principle, design, and applications," *AEU-International Journal of Electronics and Communications*, Vol. 10, 76–98, September 2019.

7. Liu, J. F., W. Tang, M. Wang, H. C. Zhang, H. F. Ma, X. Fu, and T. J. Cui, "A dual-mode UWB antenna for pattern diversity application," *IEEE Transaction on Antennas and Propagation*, Vol. 68, No. 4, 3219–3224, February 2020.
8. Singh, D., B. K. Mishra, and S. Yadav, "An UWB antenna with dual notched-band characteristics at WLAN band and X-band application," *Optical and Wireless Technologies*, 625–630, Springer, Singapore, 2020.
9. Yalduz, H., T. E. Tabaru, V. T. Kilic, and M. Turkmen, "Design and analysis of low-profile and low-SAR full-textile UWB wearable antenna with metamaterial for WBAN applications," *AEU-International Journal of Electronics and Communications*, Vol. 126, 153465, November 2020.
10. Kumar, M. and V. Nath, "A circularly polarized printed elliptical wide-slot antenna with high bandwidth-dimension-ratio for wireless applications," *Wireless Networks*, Vol. 26, No. 7, 5485–5499, June 2020.
11. Chen, Q., H. Zhang, X. L. Min, and L. C. Yang, "Compact CPW-fed dual-band linearly and circularly polarized monopole antenna for WiMAX and WLAN," *Microwave Journal*, Vol. 62, No. 5, 68–84, 2019.
12. Tran, H. H. and T. T. Le, "Ultra-wideband, high-gain, high-efficiency, circularly polarized Archimedean spiral antenna," *AEU-International Journal of Electronics and Communications*, Vol. 109, 1–7, September 2019.
13. Kumar, R. and R. K. Chaudhary, "Compact asymmetric cross-shaped rectangular dielectric resonator antenna for wideband circular polarization," *Microwave and Optical Technology Letters*, Vol. 61, No. 7, 1863–1873, July 2019.
14. Tran, H. H., N. Hussain, and T. T. Le, "Low-profile wideband circularly polarized MIMO antenna with polarization diversity for WLAN applications," *AEU-International Journal of Electronics and Communications*, Vol. 108, 172–180, August 2019.
15. Kumar, R. and R. K. Chaudhary, "Investigation of higher-order modes excitation through F-shaped slot in rectangular dielectric resonator antenna for wideband circular polarization with broadside radiation characteristics," *International Journal of RF and Microwave Computer-Aided Engineering*, Vol. 28, No. 6, August 2018.
16. Kumar, M. and V. Nath, "Dual-band dual-polarized stacked octagonal fractal patch antenna with nonlinear manipulation," *IEEE Radio and Antenna Days of the Indian Ocean (RADIO)*, 1–4, 2018.
17. Mondal, T., S. Maity, R. Ghatak, and S. R. B. Chaudhuri, "Design and analysis of a wideband circularly polarised perturbed psi-shaped antenna," *IET Microwaves, Antennas & Propagation*, Vol. 12, No. 9, 1582–1586, July 2018.
18. Tewari, M., A. Yadav, and R. P. Yadav, "Polarization reconfigurable circular patch antenna: Parasitic stub," *International Conference on Wireless Communications, Signal Processing and Networking (WiSPNET)*, 1083–1086, 2017.
19. Kumar, V. and B. Gupta, "On-body measurements of SS-UWB patch antenna for WBAN applications," *AEU-International Journal of Electronics and Communications*, Vol. 70, No. 5, 668–675, May 2016.
20. Fujita, K., K. Yoshitomi, K. Yoshida, and H. Kanaya, "A circularly polarized planar antenna on flexible substrate for ultra-wideband high-band applications," *AEU-International Journal of Electronics and Communications*, Vol. 69, No. 9, 1381–1386, September 2015.
21. Altaf, A., Y. Yang, K. Lee, and K.C. Hwang, "Circularly polarized Spidron fractal dielectric resonator antenna," *IEEE Antennas and Wireless Propagation Letters*, Vol. 14, 1806–1809, April 2015.
22. Ganguly, D., D. Guha, and Y. M. M. Antar, "Cross-finned UWB monopole for wireless applications: Design insight and characterization," *AEU-International Journal of Electronics and Communications*, Vol. 116, 153055, March 2020.
23. Garg, R. K., M. V. D. Nair, S. Singhal, and R. Tomar, "A new type of compact ultra-wideband planar fractal antenna with WLAN band-rejection," *Microwave and Optical Technology Letters*, Vol. 62, No. 7, 2537–2545, July 2020.

24. Chen, Y. and C. F. Wang, *Characteristic Modes: Theory and Applications in Antenna Engineering*, John Wiley & Sons, 2015.
25. Ylä-Oijala, P., "Generalized theory of characteristic modes," *IEEE Transactions on Antennas and Propagation*, Vol. 67, No. 6, 3915–3923, June 2019.
26. Zhang, Q., R. Ma, W. Su, and Y. Gao, "Design of a multimode UWB antenna using characteristic mode analysis," *IEEE Transactions on Antennas and Propagation*, Vol. 66, No. 7, 3712–3717, July 2018.
27. Park, D., L. Qu, and H. Kim, "Compact circularly polarised antenna utilising the radiation of the ground plane based on the theory of characteristic modes," *IET Microwaves, Antennas & Propagation*, Vol. 13, No. 10, 1509–1514, August 2019.
28. Chunling, C., "Characteristic mode analysis and design of a slot-loaded low-profile wideband microstrip patch antenna," *Microwave and Optical Technology Letters*, Vol. 62, No. 3, 1374–1379, March 2020.
29. Singh, H. V. and S. Tripathi, "Compact UWB MIMO antenna with cross-shaped unconnected ground stub using characteristic mode analysis," *Microwave and Optical Technology Letters*, Vol. 61, No. 7, 1874–1881, July 2019.
30. Quintero, G., J. F. Zurcher, and A. K. Skrivervik, "System fidelity factor: A new method for comparing UWB antennas," *IEEE Transactions on Antennas and Propagation*, Vol. 59, No. 7, 2502–2512, July 2011.
31. Kwon, D. H., "Effect of antenna gain and group delay variations on pulse-preserving capabilities of ultra-wideband antennas," *IEEE Transactions on Antennas and Propagation*, Vol. 54, No. 8, 2208–2215, August 2006.